PCCP

Study of Aluminum Oxide Films Deposited using Thermal ALD and Effect of Low Thermal Budget Annealing

Journal:	*Physical Chemistry Chemical Physics*
Manuscript ID:	CP-ART-08-2014-003430.R1
Article Type:	Paper
Date Submitted by the Author:	14-Aug-2014

Complete List of Authors:	Singh, P. K.; National Physical Laboratory, Vandana, Vandana; CSIR-National Physical Laboratory, Silicon Solar Cell Group, Physics of Energy harvestiong Division Batra, Neha; CSIR-National Physical Laboratory, Silicon Solar Cell Group, Physics of Energy harvestiong Division Gope, Jhuma; CSIR-National Physical Laboratory, Silicon Solar Cell Group, Physics of Energy harvestiong Division Singh, Rajbir; CSIR-National Physical Laboratory, Silicon Solar Cell Group, Physics of Energy harvestiong Division Panigrahi, Jagannath; CSIR-National Physical Laboratory, Silicon Solar Cell Group, Physics of Energy harvestiong Division Tyagi, Sanjay; Central Electronics Limited, Sahibabad, Pathi, P; National Physical Laboratory, Srivastava, SK; National Physical Laboratory, Rauthan, CM; National Physical Laboratory,

- Silicon surface passivation is studied using Al_2O_3 films by thermal ALD process.
- A low thermal budget process is used for annealing.
- Surface recombination velocity below 10cm/s is realized for short anneal time (~100 s).
- As-deposited and annealed films show the presence of positive fixed charges.
- Field and chemical passivation is investigated in terms of fixed charge and interface defect densities.

Study of Aluminum Oxide Films Deposited using Thermal ALD and Effect of Low Thermal Budget Annealing

Vandana*, Neha Batra, Jhuma Gope, Rajbir Singh, Jagannath Panigrahi, Sanjay Tyagi[1], P Pathi, SK Srivastava, CMS Rauthan and PK Singh*
Silicon Solar Cell Group
(Network of Institutes for Solar Energy)
CSIR - National Physical Laboratory
New Delhi-110012

Abstract

Thermal ALD deposited Al_2O_3 films on silicon show marked difference in surface passivation quality as a function of annealing time (using rapid thermal process). An effective and quality passivation is realized in short anneal duration (~100s) which is reflected in the low surface recombination velocity (SRV <10 cm/s). The deduced values are close to the best reported SRV obtained by high thermal budget process (with annealing time between 10-30 min) conventionally used for improved surface passivation. Both as-deposited and low thermal budget annealed films show the presence of positive fixed charges and has never been reported in the literature before. The role of field and chemical passivation is also investigated in terms of fixed charge and interface defect densities. Further, the importance of anneal step sequence in MIS structure fabrication protocol is also investigated from the view point of its effect on nature of fixed changes.

Key words: Surface passivation, aluminum oxide, thermal ALD, low thermal budget annealing

*Corresponding author, Email: vandana1@nplindia.org, pksingh@nplindia.org
[1]Author is working at Central Electronics Limited, Sahibabad, India.

Introduction

In a semiconductor, recombination losses occur largely via defect levels within the band gap. These defects are located within the bulk material and at the surfaces (largely due to the presence of dangling bonds). The reduction in recombination losses at semiconductor interface is of prime importance for numerous photonic devices such as light emitting diodes, photo-detectors and photovoltaic cells [1]. The losses emanating from the two surfaces can be reduced by surface passivation and is an area to be addressed for making efficient next generation semiconductor devices. Surface passivation is becoming increasingly important to enhance the performance of both single crystal (c-Si) and multi-crystalline silicon (mc-Si) solar cells [2]. In order to reduce cost of silicon solar cells made on expensive wafers (high quality silicon), thinner substrates (to reduce the usages in terms of watt/gm) are required [2, 3]. A reduction in thickness and surface modification (either by anisotropic or nano-texturisation) to reduce reflection losses lead to the increase of surface to volume ratio and, consequently, the surface recombination becomes a dominant loss factor [4]. This affects the solar cell performance parameters adversely. The passivation reduces surface recombination losses by two ways, i.e., chemical passivation (reduction of the density of electronic surface states) and field effect passivation (the presence of fixed charges in the layer over the silicon surface, such as oxides, reduces the carrier density underneath the Si/oxide interface) [1, 5-8]. A well passivated surface reduces recombination of photo-generated carriers in the vicinity of the two surfaces and improves the cell performance parameters [9-12]. Thermal silicon oxide (SiO_2), silicon nitride (a-SiN_x:H) and amorphous silicon (a-Si:H) are commonly used for surface passivation of c-Si solar cells [13-19]. Aluminum oxide (Al_2O_3), a dielectric, has excellent surface passivation properties on c-Si of both conductivity type materials [5-7]. Recently Al_2O_3 films have been used to passivate silicon surface to achieve high efficiency solar cells [9-12]. There are several methods for Al_2O_3 film

deposition, e.g., sputtering [20], atmospheric pressure chemical vapor deposition [21], RF magnetron sputtering [22] and plasma enhanced chemical vapour deposition, [23,24] etc. Atomic layer deposition (ALD) has been proven a valuable technique for the growth of Al_2O_3 thin films [25]. ALD is a conformal coating technique, by which high level of control over film thickness and uniformity can be achieved besides being a low temperature process. There are several reports related with the surface passivation property of Al_2O_3 films deposited using thermal ALD process [1, 5-7]. The measure of surface passivation is surface recombination velocity (SRV) which can be deduced from the measured minority carrier lifetime values after passivation. There are reports where as-deposited Al_2O_3 films did not exhibit high quality passivation rather a post deposition anneal is required [1, 5-7]. Normally 30 min post-deposition anneal at 400ºC is reported. To the best of our knowledge, low thermal budget annealing is very scantly reported in the literature. On the other hand, in some reports, it is observed that as deposited films show better SRV values [26] and hence attain surface passivation effect. All this indicates that the passivation mechanism is not yet fully understood and is not straight forward for as deposited and annealed films. Films reported in various studies are different in terms of deposition parameters and conditions, therefore, show different performance under as deposited and annealed state. The overall performance could be explained either individually or as a combined effect of chemical and field effect passivation which are described in terms of interface defect and fixed charge densities respectively [1, 5-7].

In this paper, study of c-Si surface passivation by Al_2O_3 film is reported. The Al_2O_3 films of different thickness are deposited at 300ºC followed by sample curing to optimize post-anneal time (t_{anl}) at a fixed annealing temperature (T_{anl}=400ºC). Effect of the film thickness on effective minority carrier lifetime values and refractive index is investigated. The minority carrier lifetime

is measured from which SRV values (at Al_2O_3/Si interface) are deduced and, hence, the effectiveness of surface passivation is evaluated. C-V measurements are used to find the flat band voltage (V_{FB}), density of fixed charges (Q_F) and interface trap (D_{it}).

1. Experimental

To grow Al_2O_3 thin films, trimethylaluminum [TMA, $Al(CH_3)_3$)] (procured from M/s SAFC, Hitech, UK) and H_2O (deionised water of 18.3 MΩ) are used as precursors for aluminum and oxygen source. The films were deposited in an ALD reactor (Model: R200, M/s Picosun, Finland). The films are grown on float zone (FZ) n- and p-Si (325±10 μm thick) substrate of (100) orientation and resistivity (5±0.5 Ωcm). The substrate temperature (T_{sub}) is fixed at 300ºC. In order to ensure exactly the same optical and electronic properties, each sample is a quarter diced from chemically mechanically polished (CMP), 100 mm diameter wafer. The samples are cleaned in piranha solution (PC, H_2SO_4:H_2O_2::4:1 solution for 15 min) followed by 2 min dip in diluted HF (5% solution). A single deposition cycle in ALD system consists of two half cycles; one TMA pulse and the other H_2O pulse and each half cycle is separated by nitrogen purge step. During each cycle, one monolayer of the material is formed and as the number of cycle progresses, number of mono-layers grows one over another. After deposition of desired thickness of the layer on one side, the sample is flipped after taking it out from the deposition chamber to load lock, in order to get film deposition on the rear side. The same thickness of the film is grown on the rear side. Samples (S_1-S_5) of various thicknesses are prepared by varying the number of deposition cycles (details are given in Table 1). Post-deposition annealing (T_{anl}) is carried out at 400°C (commonly used and optimized during the course of study) in nitrogen ambient using rapid thermal processing (RTP Model: AS-one 150, M/s Annealsys, France).

The film thickness (d_{Al2O3}) and refractive index (n_{Al2O3}) is measured by spectroscopic ellipsometer (Model: M2000, M/s J.A. Wollam Co. Inc., USA). The reflectivity of the films is measured using spectrophotometer fixed with an integrating sphere (Model: PVE 300, M/s Benthem, UK with an integrating sphere DTR6). To ensure the correctness of the measured reflectivity values, the measurements are done after base line (i.e., back ground) correction using a standard high purity $BaSO_4$ powder pressed in the form of a pallet. Fourier transform infrared spectroscopy (Model 2000, M/s Perkin Elmer spectrometer, USA) is used to get information about the surface bonding.

Minority carrier lifetime (τ_{eff}) is measured using photo-conductance decay method (Model: WCT-120, Sinton lifetime tester) and the uniformity of τ_{eff} is examined by mapping of lifetime parameter using microwave photoconductive decay system (μW-PCD, Model: WT 2000, M/s Semilab Zrt, Hungary). τ_{eff} measured by Sinton's lifetime tester is an effective average value of carrier lifetime. In this tool, excess carriers are generated by a flash and the sheet conductivity is measured by RF coil inductively coupled to sample. The flash intensity and sheet conductivity are converted into generation rate of electron-hole (e-h) pairs and the average excess carrier density by using mobility model [27]. The injection levels (Δn) can be varied in a wide range ($10^{13}<\Delta n<10^{16}$ cm^{-3}). The system operates in (i) quasi steady state photo-conductance, QSSC (ii) transient photo-conductance (TPC) decay modes. In the QSSC, decay constant of the flash should be at least 10 times slower than the carrier lifetime so that excess carrier's population attains steady state and hence, the lifetime is measured in steady state condition. In the transient mode, fast pulse of light which peaks and decays back in ~15 μs is used and the photo-conductance decay is measured to determine effective carrier lifetime. This mode is suitable for high lifetime materials. Transient mode is used when the measured lifetime

values are more than 200μs and quasi steady state mode is used in low lifetime material [28]. The measurements are also made using μW-PCD where a 904 nm pulsed laser (penetration depth ~30 mm) and a microwave source operating at 10GHz are used. The former is for optical excitation and the latter for signal detection (where decay of excess carrier concentration is monitored by the microwave reflectance). However, the measured τ_{eff} by the WCT-120 and the μW-PCD could be compared at the same injection levels [29].

Metal-insulator-semiconductor (MIS) structure (schematic of which is given in Fig. 1) is fabricated by depositing aluminum dots (areas~ 0.02cm^2) using an e-beam evaporation system (M/s Hind Hivac, India). The capacitance-voltage (C-V) measurements are performed with an impedance/gain phase analyzer (Model: 1260, M/s Solartron, UK).

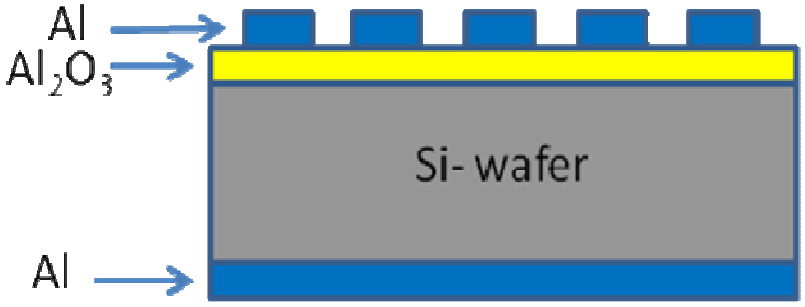

Figure 1

2. Results and Discussion

2.1 Film thickness and refractive index

The AFM and SEM studies reveal that the ALD deposited films are highly conformal and uniform. A typical atomic force micrograph of S3 is given in Fig. 2. The RMS surface roughness is ~5 Å which is almost the same as that of the substrate (chemically mechanically polished silicon wafer) within measurement uncertainty.

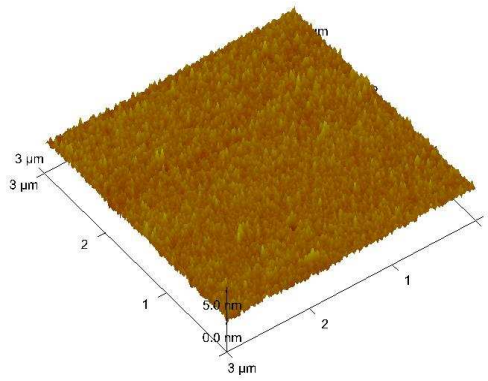

Figure 2

The measured film thickness and refractive index as a function of number of deposition cycles is shown in Fig. 3. A linear growth (@0.09 nm/cycle) of film thickness as a function of number of process cycles is seen which is indicative of highly controlled film growth. The refractive index also changes with the number of cycle and increases with increase in film thickness. Refractive index values are rather low at lower film thicknesses and stabilizes for d_{Al2O3} ~30nm. The ellipsometric measurements are sensitive to a perturbation parameter at low thicknesses [30]. In the reported values, this aspect is taken care by the error bars. The measured d_{Al2O3} and n_{Al2O3} values are effective values rather than the true estimation of the parameters.

Although Al_2O_3 is thermodynamically stable on silicon, however, growth of a SiO_2 or an aluminum silicate layer at the Al_2O_3/Si interface is inevitable as the growth occurs under non-equilibrium conditions [25]. It is observed that initially the thickness of the interfacial layer increases and stabilizes at 1-2 nm [5, 25] during Al_2O_3 layer growth. The interfacial layer affects the refractive index and the measured n_{Al2O3} may be that of Al_2O_3/SiO_2 composite layer. The low refractive index for thinner Al_2O_3 ALD film thicknesses is attributed to this interfacial layer. Once the thickness of interfacial layer stabilizes, the value of n is close to the refractive index of

bulk alumina (~1.77) within measurement error and the measured value is close to the values reported in ALD deposited Al_2O_3 films [25]. The annealing of the films does not change either thickness or refractive index. This further reiterates the conformity and compactness of the thermally grown films. The typical monolayer thickness of Al_2O_3 is 0.3 nm and growth rate 0.09 nm/cycle is quite low, albeit similar growth rates are given in the literature too [25].

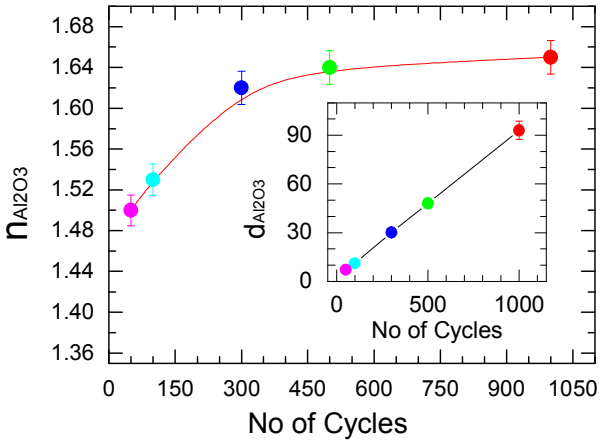

Figure 3

2.2 Reflectivity

Figure 4 shows spectral dependence of the reflectivity (R_λ) of samples S_1-S_4 along with that of reference CMP silicon wafer. It is observed that surface reflectivity does not change much at lower thickness (<10nm) and is close to the value of CMP sample, but increase in d_{Al2O3} reduces R_λ. An overall reduction in R_λ is observed in 400 to 1050 nm range. However, minima of R_λ shifts from ~400 nm to ~600 nm with change in film thickness from ~30 nm to ~93 nm. The average reflectance reduces from 32.8% (CMP-Si) to 32.13%, 27.98%, 21.4%, and 16.8% respectively for samples S_4, S_3, S_2 and S_1. The minimum R_λ is ~4% for sample S_1. This trend is expected in single layer coating.

The position (wavelength, λ_{min}) of minimum in R_λ is related to the thickness and the refractive index by the relation; $\lambda_{min} = 4d_{Al2O3}*n_{Al2O3}$ [31, 32]. On the other hand, in the regions away from λ_{min}, a combined effect of constructive (i.e., $2d_{Al2O3}*n_{Al2O3} / \lambda=2\pi$) and destructive (i.e., $2d_{Al2O3}*n_{Al2O3} / \lambda=\pi$) interference prevails depending on the path length (extent of d_{Al2O3} and n_{Al2O3} values) that decides the magnitude of R_λ [31-33]. For example, the value of λ_{min} is estimated using the measured d_{Al2O3} (=93 nm) and n_{Al2O3} (=1.65) and is found to be 614 nm for sample S_1. This value is the same (= 630 ±2.5% nm) measured by spectroscopic measurement in S_1 within measurement uncertainty. The shift in λ_{min} position is the manifestation of the change in d_{Al2O3} and n_{Al2O3}. It can be noted that there is a systematic change in R_λ with the increase in thickness of the film particularly in 450 to 1000 nm range.

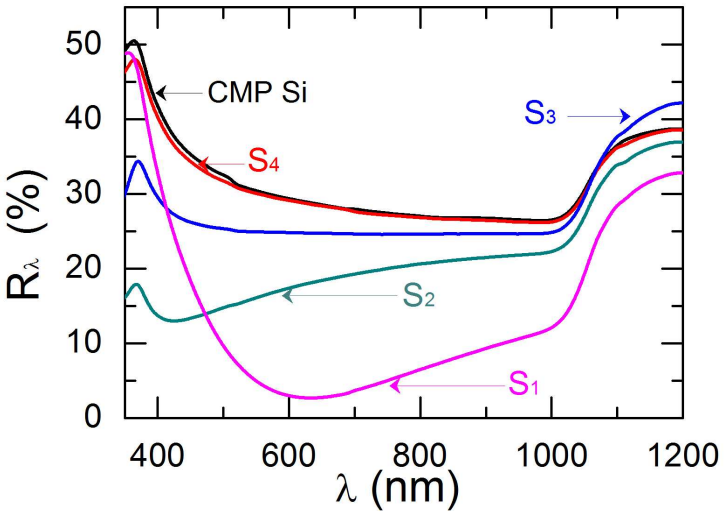

Figure 4

Although ALD is generally adopted to deposit ultra thin films, but reflectivity studies are carried out to see the effect of film thickness and their potential to work as antireflection coating (ARC) in conjunction with passivation properties.

3.3 FTIR spectroscopy

Figure 5 shows the transmittance FTIR spectra of sample S_1-S_4. The broad absorption band in the range of 600-400 cm^{-1} is attributed to the Al-O stretching in the characteristic spectra of Al_2O_3. It is reported that a band at 564 cm^{-1} results from two unresolved structures at 562 and 565 cm^{-1}. The first one is assigned to Al–O bending for AlO_6 (5+1), while the second is a pure Al–O stretching mode for AlO_4 [34]. The peak observed in 560-570 cm^{-1} region (a minor shift with d_{Al2O3}) represents Al–O modes. On the other hand, the observed peak in 670-700 cm^{-1} may be attributed to Al-O stretching mode [35, 36]. The absorption peak at ~710 cm^{-1} correspond to the Al-O stretching mode, respectively [35, 36]. The peak at 1040-1060 cm^{-1} corresponds to Si-O-Si [35]. An absorbance peak due to Al=O at ~1345 cm^{-1} (as shown in the inset of the figure) is also present [37] but is rather weak whereas in some other reports this peak is absent [35]. In all the samples, FTIR spectra show characteristic peaks of Al_2O_3.

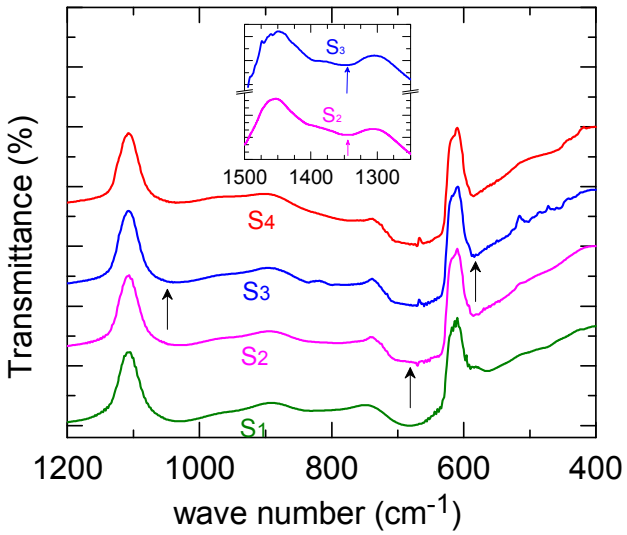

Figure 5

3.4 Minority Carrier Lifetime:

The measured minority carrier lifetime value has contributions from the bulk (τ_b) and recombination lifetime (τ_s) associated with the wafer surfaces which are related as [29, 38];

$$\frac{1}{\tau_{eff}} = \frac{1}{\tau_b} + \frac{1}{\tau_s}$$

where τ_s is equal to $(D_p\beta^2)^{-1}$ and which in turn related to surface recombination velocity S through the relation $\beta \tan(\beta d/2) = S/D_p$. In the case of high lifetime material, measured τ_{eff} is predominantly a measure of surface recombination.

To evaluate the surface passivation, the upper limit of S_{eff} is determined from the effective lifetime at an injection level (Δn) at 10^{15} cm^{-3} by assuming large bulk lifetime and, therefore, gives the worst estimate of SRV value. Fig. 6 gives typical photo-conductive decay curve obtained by Sinton's lifetime tester in transient mode.

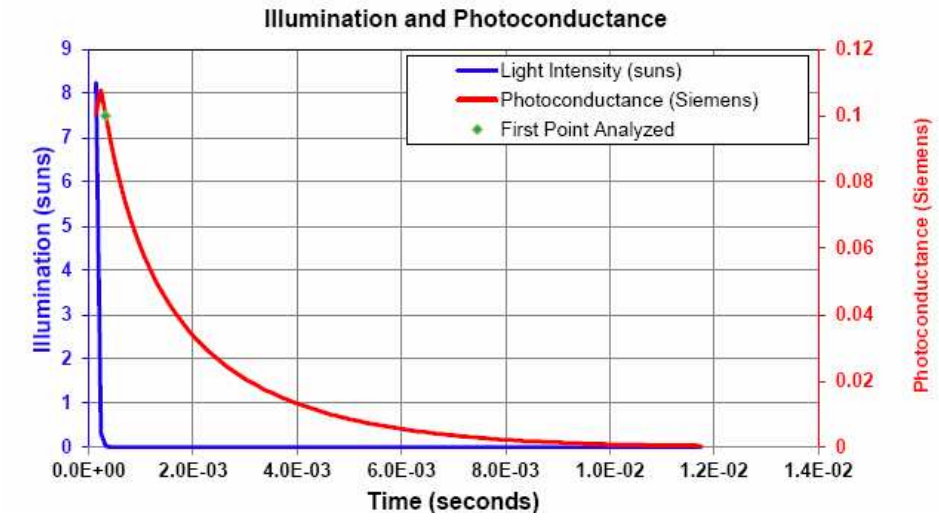

Figure 6

It is known that annealing conditions play an important role in surface passivation performance. To optimize the film annealing conditions, rapid thermal processing technique (RTP) is used which is a low thermal budget process. For a given set of experiment, annealing temperature is fixed at 400ºC and annealing time (t_{anl}) is varied.

Figures 7 (a), (b) and (c) show effective minority carrier lifetime (τ_{eff}) data as a function of injection level for as deposited and annealed samples S_2, S_3 and S_4 respectively for different annealing time (t_{anl}) at fixed T_{anl}=400ºC. Lifetime data shows a good quality passivation in the entire injection level range ($5x10^{13}$ to $1x10^{16}$ cm^{-3}) for all the three samples. The value of τ_{eff} in un-passivated samples is 18 and 1.5 μs for n- and p-Si respectively which is controlled by τ_s (that is high SRV $>10^3$ cm/s in Table 2, and $>10^4$ cm/s in [39]). An interesting observation is that the measured τ_{eff} values increases for shorter sintering time duration, reaches a peak value in the vicinity of 100 s and on further increase in t_{anl}, the value of τ_{eff} start decreasing. The optimized sintering time for the best passivation is 105 s. It is to be noted that in most of the publications [1, 5-8, 25], annealing is done for longer time duration (10-30 min) and there is hardly any publication for shorter t_{anl}.

Table 2 summarizes the measured minority carrier lifetime and corresponding estimated SRV values with films of different thicknesses. It is observed that increase in film thickness improves the surface passivation and a good surface passivation is realized in as deposited thick films. For example, the lowest SRV values (<10cm/s) is obtained in sample S_1 (Table 1, n-Si). Similar trend is observed in both n and p-Si. Surface recombination velocity values for S_2, S_3 and S_4 samples with anneal duration shows minimum at ~105s and the SRV increases both at lower and higher t_{anl} as can be seen from Fig. 8. Figure 9 gives an idea about the uniformity of τ_{eff} over the sample area where mapping of τ_{eff} using μ-PCD method is shown for sample S_3.

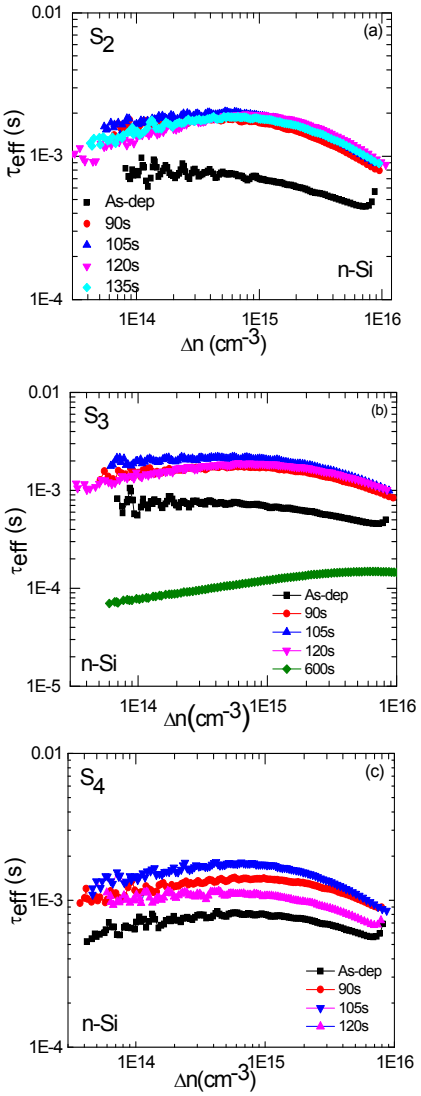

Figure 7

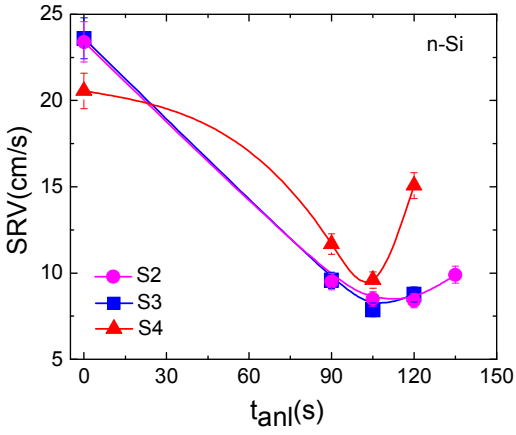

Figure 8

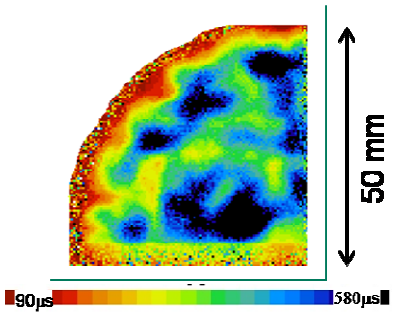

Figure 9

3.7 Capacitance-Voltage measurements: Effect of annealing sequence

Capacitance measurement as a function of voltage (C-V) is very important because it gives vital information about the passivation at Al_2O_3/Si interface [1, 5-8]. MIS structure is used for C-V measurements where there is an important step of metal contacts formation. Two different experiments (i.e., Post and pre-anneal prior to metal contact formation) were carried out to see the effect of annealing step on C-V characteristics. MIS structure is made by creating polka dot pattern of Al over the Al_2O_3 film as described under "Experimental". In the first experiment annealing step (10min in N_2 ambient) is done after depositing Al metal whereas in the second experiment the Al_2O_3 film was annealed (10min in N_2 ambient) prior to the formation of metal contacts. The former is referred as S_{MF} and the later as S_{AF} in the subsequent text. Figure 10 shows the C-V data for an as-deposited and the two annealed samples; S_{MF} and S_{AF}.

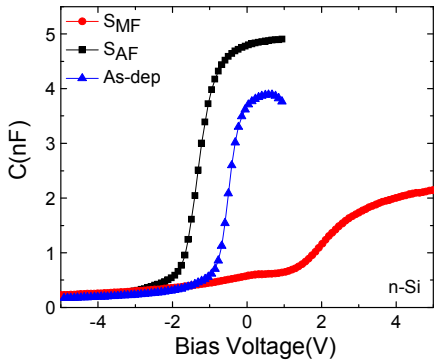

Figure 10

There is decrease in oxide capacitance in S_{MF} sample in contrast to increase in oxide capacitance with S_{AF} condition. Another important observation is that flat band voltage position is opposite in the two cases. In the sample, where annealing is done prior to metal deposition (S_{AF}) shows positive charges activation. Contrary to this, activation of negative charges occurs when contacts are made prior to anneal (S_{MF}). When aluminum contact is made on the Al_2O_3 films and subsequent annealing (S_{MF}), Al metal may diffuse into the aluminum oxide film that may cause decrease in the capacitance. On the other hand, when Al_2O_3 film is annealed prior to formation of metal contacts (S_{AF}), and therefore no high temperature step is involved after metal deposition. In this case the possibility of Al diffusion into Al_2O_3 is completely ruled out. Consequently, higher capacitance is measured and the C-V data provides better idea about the films and interface properties. Therefore, in the C-V study, the protocol of S_{AF} is followed.

As mentioned earlier that silicon surface passivation using Al_2O_3 films owes to the combined effect of field and chemical which is described in terms of fixed charge density and interface defect density respectively. Field effect passivation is provided by fixed charges located near the Si/Al_2O_3 interface. Chemical passivation is attributed to hydrogenation at interface, film relaxation, Si-O bond rearrangement or additional oxide growth which may work individually or in combination [25]. Figure 11 shows normalized C-V curves of MIS structures made on as deposited and annealed Al_2O_3 films (t_{anl} = 90, 105, 120 and 600s) on S_3 (d_{Al2O3}~30nm).

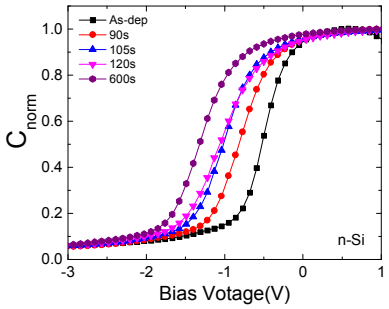

Figure 11

The measurements are carried out at 1 MHz frequency. A negative shift in C-V curve with annealing confirms activation of positive fixed charges in Al_2O_3 film also reported in literature [40]. Low thermal annealing is not very well explored besides the post-anneal activation of positive (+ve) charges. Only few publications reported activation of positive charges. Further, the film capacitance increases with annealing as compared to as deposited sample. Table 3 compiles the parameters extracted from C-V measurement data. Fixed charge density calculated using flat band shift shows an increase in Q_F with t_{anl} from $0.36x10^{12}$ cm^{-2} to $1.34x10^{12}$ cm^{-2} whereas interface defect density, D_{it}, decreases from $2.96x10^{12}eV^{-1}cm^{-2}$ to $1.5x10^{12}eV^{-1}cm^{-2}$ with t_{anl} variation from 0 to 120s. It is reasonable to assume that both chemical and field effect co-exist in Al_2O_3 surface passivation. A change in D_{it} and Q_F values with t_{anl} gives indication that the two effects work in tandem. An increase in Q_F with t_{anl} is observed till 120 s followed by marginal decrease thereafter. An opposite trend is observed in D_{it} values. The best results (maximum τ_{eff} and the lowest SRV) could be obtained in the range where Q_F is maximum and D_{it} is minimum. In the present case, maximum and minimum values of Q_F and D_{it} are equal to $1.34x10^{12}$ cm^{-2} and $1.4x10^{12}$ eV^{-1} cm^{-2} respectively corresponding to t_{anl} 120 s and 105 s respectively. Therefore, the best τ_{eff} or SRV could be realized at t_{anl} between 105 and 120 s. But for larger annealing duration (>180s), the Q_F is practically the same and D_{it} degrades which results in an effective decrease in τ_{eff}. For 600s annealing, although Q_F is higher which is rather surprising as compared to the value obtained after 120s annealing, but D_{it} also become large (twice compared to the value corresponding to 120s). The two acts in opposite directions and therefore net effect is degradation in passivation performance (as could be seen in Fig. 7(b)). The magnitude of Q_F gets altered after annealing in either direction. On the other hand, D_{it} is expected to rise if the passivating species (attached to silicon surface or at the interface) get

detached with the increase in annealing time. Therefore, the quality of surface passivation is a trade-off between field effect and chemical passivation and the best passivation (maximum τ_{eff} or minimum SRV) could be realized when Q_F and D_{it}, the two quantifying parameters, attain their respective highest and lowest values at the same annealing temperature. Further, the presence of positive charges may be attributed to the existence of Al interstitials and O vacancies. This is in good agreement with the ionic nature of the Al_2O_3 [1, 8]. This reconfirms the origin of positive charges for low thermal budget annealed Al_2O_3 films with low SRV.

Conclusions

Silicon surface passivation is studied using Al_2O_3 thin films of various thicknesses deposited on silicon substrate at 300ºC. The τ_{eff} values show improvement in surface passivation which is also reflected in SRV values and reflectivity measurements show its utility as antireflection coating. C-V measurement data shows the importance of annealing step sequence in determining true information about the deposited films. The optimization of process parameters of Al_2O_3 film reveals that 105 s anneal time gives best passivation results at 400ºC wherein $Q_F = 1.22 \times 10^{12}$ cm^{-2} and $D_{it} = 1.4 \times 10^{12}$ eV^{-1} cm^{-2}. Therefore, the best surface passivation (maximum τ_{eff} or minimum SRV) could be obtained for annealing time in the vicinity of 100 s and indeed is a trade-off between field effect (high Q_F) and chemical passivation (low D_{it}). Low thermal budget process (like rapid thermal anneal) activates positive fixed charges (as confirmed by C-V data measurements). The presence of positive charges reiterates the existence of Al interstitials and O vacancies, the primary mechanism for surface passivation of crystalline silicon.

Acknowledgement

The work was carried out under NWP-55 grant from Council of Scientific and Industrial Research, India under TAPSUN initiative. NB also thanks to CSIR for the research fellowship.

References

1 B. Hoex, J. J. H. Gielis, M. C. M. van de Sanden, and W. M. M. Kessels, J. Appl. Phys., **2008**, 104, 113703 (7 pages).

2 A. G. Aberle, Progress in Photovoltaics: Research and Applications, 2000, 8, 473-487.

3 International Technology Roadmap for Photovoltaic (ITRPV) 2014; http:www.**itrpv**.net

4 B. Hoex, A. J. M. van Erven, R. C. M. Bosch, W. T. M. Stals, M. D. Bijker, P. J. van den Oever, W. M. M. Kessels, and M. C. M. van de Sanden, Prog. Photovoltaics, **2005**, 13, 705-712.

5 B. Hoex, S. B. S. Heil, E. Langereis, M. C. M. van de Sanden, and W. M. M. Kessels, Appl. Phys. Lett., **2006**, 89, 042112 (3 pages).

6 G. Agostinelli, A. Delabie, P. Vitanov, Z. Alexieva, H. F. W. Dekkers, S. DeWolf, and G. Beaucarne, Sol. Energy Mater. Sol. Cells, **2006**, 90, 3438-3443.

7 B. Hoex, J. Schmidt, P. Pohl, M. C. M. van de Sanden, and W. M. M. Kessels, J. Appl. Phys, **2008**, 104, 044903 (12 pages).

8 K. Matsunaga, T. Tanaka, T. Yamamoto, and Y. Ikuhara, Phys. Rev. B, 2003, **68**, 085110 (9 pages).

9 P. Saint-Cast, D. Kania, M. Hofmann, J. Benick, J. Rentsch, and R. Preu, Appl. Phys. Lett., **2009**, 95, 151502 (3 pages).

10 J. Benick, B. Hoex, M. C. M. van de Sanden, W. M. M. Kessels, O. Schultz, and S. W. Glunz, Appl. Phys. Lett., **2008**, 92, 253504 (3 pages).

11 P. Saint-Cast, J. Benick, D. Kania, L. Weiss, M. Hofmann, J. Rentsch, R. Preu, and S. W. Glunz, IEEE Electron Device Lett. **2010**, 31, 695-697.

12 B. Liao, R. Stangl, T. Mueller, F. Lin, C. S. Bhatia, and B. Hoex, J. Appl. Phys., **2013**, 113, 024509 (5 pages).

[13] J. Schmidt and A. Cuevas, J. Appl. Phys., **1999**, 85, 3626-3633.

[14] M. J. Kerr and A. Cuevas, Semicond. Sci. Technol., **2002**, 17, 166-172.

[15] S. de Wolf, G. Agostinelli, G. Beaucarne, and P. Vitanov, J. Appl. Phys., **2005**, 97, 063303 (8 pages).

[16] M. Schaper, J. Schmidt, H. Plagwitz, and R. Brendel, Prog. Photovoltaics, **2005**, 13, 381-386.

[17] T. F. Schulze, H. N. Beushausen, C. Leendertz, A. Dobrich, B. Rech, and L. Korte, Appl. Phys. Lett., **2010**, 96, 252102 (3 pages).

[18] S. de Wolf, B. Demaurex, A. Descoeudres, and C. Ballif, Phys. Rev. B, **2011**, 83, 233301-233304.

[19] A. Illiberi, M. Creatore, W. M. M. Kessels, and M. C. M. van de Sanden, Phys. Status Solidi (RRL), **2010**, 4, 206-208.

[20] T. A. Li, S. Ruffell, M. Tucci, Y. Mansoulié, C. Samundsett, S. De Iullis, L. Serenelli, and A. Cuevas, Sol. Energy Mater. Sol. Cells, **2011**, 95, 69-72.

[21] K. O. Davis, K. Jiang, M. Wilson, C. Demberger, H. Zunft, H. Haverkamp, D. Habermann, and W. V. Schoenfeld, Physica Status Solidi (RRL), **2013**, 7, 942-945.

[22] T.-T. Li and A. Cuevas, Phys. Status Solidi (RRL), **2009**, 3, 160-162.

[23] C. Cibert, H. Hidalgo, C. Champeaux, P. Tristant, C. Tixier, J. Desmaison, and A. Catherinot, Thin Solid Films, **2008**, 516, 1290-1296.

[24] M. T. Seman, D. N. Richards, P. Rowlette, and C. A. Wolden, Chem. Vap. Deposition, **2008**, 14, 296-302.

[25] G. Dingemans and W. M. M. Kessels, J. Vac. Sci. Technol. A, **2012**, 30, 040802 (27 pages).

[26] J. Wang, S. S. Mottaghian and M. F. Baroughi, IEEE transactions on Electron Devices, **2012**, 59, 342-348.

[27] R. Lago-Aurrekoetxea, I. Tobías, C. del Cañizo, and A. Luque, Journal of the Electrochemical Society, **2001**, 148, G200-G206.

[28] C. Berge, J. Schmidt, B. Lenkeit, H. Nagel, and A.G. Aberle, 2nd World Conference on Photovoltaic Solar Energy Conversion, **1998**, 1426-1429.

[29] N. Batra, Vandana, S. Kumar, M. Sharma, S.K. Srivastava, P. Sharma, and P.K. Singh, Sol. Energ. Mat. Sol. Cells, **2012**, 100, 43-47.

[30] J. Lekner, "**Theory of Reflection of Electromagnetic and Particle Waves**" in Series: Developments in Electromagnetic Theory and Applications, Vol. 3, Springer Science Media Busniss BV (ISBN 978-94-015-7748-9)

[31] A. Nussbaum and R. A. Phillips, Contemporary Optics for Scientists and Engineers (Englewood Cliffs, NJ: Prince- Hall, 1974).

[32] J. Zhao and M.A. Green, IEEE transactions on Electron Devices, **1991**, 38, 1925.

[33] Vandana, N. Batra, P. Kumar, P. Sharma, P.K. Singh, Mat. Chem. Phys., 2014, 144, 242

[34] L. Favaro, A. Boumaza, P. Roy, J. Lédion, G. Sattonnay, J.B. Brubach, A.M. Huntz, R.Tétot, J. Solid State Chem, 2010, 183, 901–908

[35] R. Katamreddy, R. Inman, G. Jursich, A. Soulet, and C. Takoudis, J. of Electrochem. Society, **2006**, 153(10), C701-C706.

[36] M. Ben Rabha, M. Salem, M. A. Khakani, B. Bessais, and M. Gaidi, Mater. Sci. and Eng. B, 2013, http://dx.doi.org/10.1016/j.mseb.2012.11.021.

[37] Zivit Katz-Tsameret, Avi Raveh, J. Vac. Sci. Technol. A, 1995, 13, 1121-27

[38] A.W. Stephens, M.A. Green, Sol. Energ. Mat. Sol. Cells, **1997,** 45, 255-265.

[39] S. Kumar, P.K. Singh, S.R. Dhariwal, Appl. Phys. Lett., **2010**, 96, 162109-162111.

[40] B. Shin, J. R. Weber, R. D. Long, P. K. Hurley, C. G. Van de Walle, and P. C. McIntyre, Appl. Phys. Lett., **2010**, 96, 152908 (3 pages).

Table 1: Details of samples: The number of precursor cycles and corresponding film thickness (d_{Al2O3}) along with refractive index. (n_{Al2O3}) of Al_2O_3 made on n-Si.

Sample	No. of cycles	Thickness (nm)	Refractive Index
S_1	1000	93.1	1.65
S_2	500	48.0	1.64
S_3	300	30.1	1.62
S_4	100	11.2	1.53
S_5	50	7.2	1.5

Table 2: Measured minority carrier lifetime (τ_{eff}) and the worst estimate of surface recombination velocity (SRV) values for as deposited samples, at injection level, $\Delta n = 1\times10^{15}cm^{-3}$. The values of τ_{eff} and SRV have ~4% error in their estimation.

Sample	n-Si		p-Si	
	τ_{eff} (μs)	(cm/s)	τ_{eff} (μs)	SRV(cm/s)
Bare	18	903	1.5	10833
S_1	2244	7	820	20
S_2	1102	15	678	24
S_3	824	20	430	38
S_4	471	35	337	48
S_5	103	158	149	109

Table 3: Fixed charge density (Q_F) and interface defect density (D_{it}) in as deposited & sintered sample S_3, T_{sint}=400ºC, n-Si substrate

T_{anl}(s)	Q_F ($\times10^{12}$) cm^{-2}	D_{it} ($\times10^{12}$) states/eVcm^2
0	0.36	2.96
90	0.91	1.8
105	1.22	1.4
120	1.34	1.5
180	0.93	2.3
300	0.96	3.5
600	1.59	3.3

Figure Captions:

Figure 1: Schematic of the MIS structure.

Figure 2: AFM micrograph of S_3.

Figure 3: Refractive index as a function of number of cycles. The inset shows film thickness with number of cycles.

Figure 4: Reflectivity of samples S_1-S_4 along with bare CMP wafer.

Figure 5: FTIR spectra of samples S_1-S_4. The inset shows an absorbance peak at ~1345 cm^{-1} due to Al=O.

Figure 6: A typical photo-conductive decay curve obtained by Sinton's lifetime tester in transient mode.

Figure 7: The measured minority carrier lifetime (τ_{eff}) as a function of injection level (Δn) for n-Si samples, t_{dep}=300ºC and T_{anl}=400ºC, (a) S_2, as deposited and 90, 105, 120 and 135s annealed (b) S_3, as deposited and 90, 105, 120 and 600s annealed (c) S_4, as deposited and 90, 105 and 120s annealed.

Figure 8: SRV as a function of sintering time (t_{anl}) for sample S_2, S_3 and S_4. T_{anl}=400ºC.

Figure 9: μ-PCD lifetime map of Sample S_3. Figure shows passivation uniformity across the wafer.

Figure 10: Capacitance-Voltage curves for S_3, as deposited and the two annealed samples; S_{MF} and S_{AF} at 1MHz frequency.

Figure 11: Normalized CV curves for as deposited and annealed films at 90s, 105s, 120s and 600s at 1MHz frequency.